Calcium Copper−Titanate Thin Film Growth: Tailoring of the Operational Conditions through Nanocharacterization and Substrate Nature Effects

Raffaella Lo Nigro,*,† Roberta G. Toro,‡ Graziella Malandrino,*,‡ Ignazio L. Fragalà,‡ Maria Losurdo,*,§ Michelaria M. Giangregorio,§ Giovanni Bruno,§ Vito Raineri,† and Patrick Fiorenza‡

Institute for Microelectronics and Microsystems, IMM-CNR, Stradale Primosole n 50, 95121 Catania, Italy, Dipartimento di Scienze Chimiche, Università di Catania, INSTM UdR Catania, Viale A. Doria 6, 95125 Catania, Italy, and Institute of Inorganic Methodologies and of Plasmas, IMIP-CNR and INSTM UdR Bari, via Orabona 4, 70125, Bari, Italy

Received: April 26, 2006; In Final Form: July 11, 2006

A novel approach based on a molten multicomponent precursor source has been applied for the MOCVD fabrication of high-quality $CaCu_3Ti_4O_{12}$ (CCTO) thin films on various substrates. The adopted in situ strategy involves a molten mixture consisting of $Ca(hfa)_2$·tetraglyme, $Ti(tmhd)_2(O\text{-}iPr)_2$, and $Cu(tmhd)_2$ [Hhfa = 1,1,1,5,5,5-hexafluoro-2,4-pentanedione; tetraglyme = 2,5,8,11,14-pentaoxapentadecane; Htmhd = 2,2,6,6-tetramethyl-3,5-heptandione; O-*i*Pr = isopropoxide] precursors. Film structural and morphological characterizations have been carried out by several techniques [X-ray diffraction (XRD), scanning electron microscopy (SEM), transmission electron microscopy (TEM)], and in particular the energy filtered TEM mapping and X-ray energy dispersive (EDX) analysis in TEM mode provided a suitable correlation between nanostructural properties of CCTO films and deposition conditions and/or the substrate nature. Correlation between the nanostructure and optical/dielectric properties has been investigated exploiting spectroscopic ellipsometry.

Introduction

Perovskite oxides are widely used in many technological applications because of their high dielectric constant (ϵ) values, which open up new possible miniaturization of microelectronics devices. In particular, capacitor applications require highly insulating materials and the increasing of smaller and faster microelectronics devices is associated with similarly higher ϵ values. In the last three decades, device miniaturization has been assured by a "conservative" approach through well-established process technologies. Nevertheless, upon approaching the physical limits of conventional technologies, new and even more complex phenomena become evident and a large number of experimental and theoretical studies are, as a consequence, desired.

Recently, pioneering studies on the perovskite related calcium copper titanate, $CaCu_3Ti_4O_{12}$ (CCTO), have demonstrated that this material possesses an impressive dielectric constant value of 10^5 working at 1 MHz, which remains constant in the 100−600 K temperature range and depends slightly on work frequency in the 10^2-10^5 Hz range.[1−3] In addition, CCTO does not show ferroelectric transition or relaxor behavior. These intriguing properties render the CCTO material a real attractive alternative to the currently used ferroelectrics which in turn possess lower dielectric constant values having a stronger temperature dependence.

The central question is now whether the large dielectric response is intrinsic to a perfect crystal of CCTO or extrinsic since it may originate from defects, inhomogeneities, etc.[4−7] Some theories correlate the CCTO high ϵ value to its peculiar crystal structure.[8−11] The cubic perovskite CCTO contains square-planar Cu atoms which cause tilting of the TiO_6 octahedra. The site symmetry for Ti^{4+} in CCTO is much lower than that in cubic standard ABO_3 perovskite so that the high permettivity may arise from the local dipole moments associated with off-center displacement of Ti ions. Moreover, the tilt of the TiO_6 octahedra is large enough to accommodate local distortion, which in turn would effectively rule out the pure ferroelectric behavior.

Further explanation of such high dielectric constant can be discussed in terms of a barrier-layer mechanism related to the ceramic microstructure. Impedance spectroscopy studies on CCTO ceramic suggested an explanation for the behavior of CCTO in terms of conducting grains and insulating grain boundaries.[5] In this perspective, it can be of great importance to study and compare bulk and thin film properties. Fabrication of thin films now becomes a required issue to understand their properties and evaluate potentialities for device integration.

Some research groups have grown CCTO films on perovskite oxide substrates by pulsed laser deposition technique,[12−15] while others explored the possibility of growing CCTO films on technological substrates consisting of platinum electrode on silicon.[16−18]

Our successful metalorganic chemical vapor deposition (MOCVD) of highly epitaxial CCTO thin films on (100) $LaAlO_3$ substrates[19] still remains unique and, very recently, it has been implemented into the fabrication of CCTO films on substrates of industrial interest, namely the $Pt/TiO_2/SiO_2/Si(100)$ multilayer stack,[20] which is widely used as a bottom electrode for dielectric films.

In this paper, we report a fully comprehensive MOCVD study of the CCTO fabrication on various substrates, such as $LaAlO_3$ (100), $SrTiO_3$ (100) single crystals, and technological Pt/TiO_2/

* To whom correspondence should be addressed. E-mail: raffaella.lonigro@imm.cnr.it; gmalandrino@dipchi.unict.it; maria.losurdo@ba.imip.cnr.it.

† Institute for Microelectronics and Microsystems.

‡ Università di Catania.

§ Institute of Inorganic Methodologies and of Plasmas.

10.1021/jp062559c CCC: $33.50
Published on Web 08/16/2006

SiO_2/Si(100) multilayer. In particular, the aim of this paper is manyfold in the perspective of highlighting the multiform issues associated with the synthesis and properties of CCTO thin films. Therefore, the intriguing properties of a multicomponent (Ca, Cu, Ti) molten single source are first scrutinized to prove that this molten precursor mixture possesses suitable stability during vaporization and fast mass transport capability. Second, details of the reproducible MOCVD process for the preparation of CCTO thin films on various substrates are proposed and chemical, structural, and morphological characterization of CCTO thin films provided. Finally, the dielectric and optical properties of CCTO polycrystalline samples are accurately evaluated by ellipsometric measurements and correlated to the chemical composition and nanostructure of the deposited materials.

Experimental Section

A horizontal hot-wall MOCVD reactor was used for deposition experiments. A multimetal source consisting of a 1:1:3 mixture of $Ti(tmhd)_2(O\text{-}iPr)_2$, $Ca(hfa)_2$·tetraglyme, and $Cu(tmhd)_2$ precursors was used. The $Ti(tmhd)_2(O\text{-}iPr)_2$ and $Cu(tmhd)_2$ precursors were purchased from Aldrich Chemicals. The first was used without further purification, while the second was sublimed at 150 °C/0.1 Torr. Finally, the synthesis of the $Ca(hfa)_2$·tetraglyme adduct was realized in our laboratory as described elsewhere.[21]

Thermogravimetric analyses were performed with a Mettler Toledo TGA/SDTA 851^e analyzer under purified nitrogen flow fed into the working chamber at 60 sccm. Isothermal TG experiments were made in the 90−140 °C range. Temperatures were kept constant and measured with an accuracy of ±0.1 °C. Isotherm temperatures were reached adopting a 5 deg/min heating rate. Thermal investigations were carried out at 20 and 760 Torr. DSC measurements were made with a Mettler 3000 system equipped with a TC 10 processor and DSC 30 calorimeter. Weights of the samples were between 8 and 15 mg. Analyses were made under prepurified nitrogen with a 5 deg/min heating rate.

Ca−Cu−Ti matrices were deposited on these substrates at 600 °C. The single source reservoir was an alumina boat placed inside the reactor in the sublimation zone, maintained at a temperature of 115 °C. Mass transport to the deposition zone of the multielement source was prompted by a 100 sccm argon gas stream. A 200 sccm oxygen gas flow was introduced near the substrate surface as reacting gas. Their mass flows were controlled with 1160 MKS flowmeters, using an MKS 147 electronic control unit (±1 sccm accuracy). Depositions were carried out for 120 min, and the reactor chamber was maintained at 4 Torr during the growth process. Once the source supply was stopped, an in situ annealing process was carried out in the 750−900 °C range for 120 and 30 min in an oxygen atmosphere. Finally, the CCTO films were slowly cooled to room temperature.

$\theta-2\theta$ X-ray diffraction (XRD) patterns and rocking curve measurements were recorded on a Bruker-AXS D5005 $\theta-\theta$ X-ray diffractometer, using Cu K_α radiation, operating at 40 kV and 30 mA. Film surface morphologies were examined with use of a LEO Iridium 1450 scanning electron microscope (SEM). Film atomic composition was determined by energy-dispersive X-ray analysis (EDX) with an IXRF detector. CCTO as-deposited and annealed films were also investigated by transmission electron microscopy (TEM: JEOL 2010 F, equipped with the Gatan imagining filter, instruments). All the EF-TEM chemical maps have been acquired by the three windows method.

Ellipsometric spectra were acquired in the photon energy range 0.75−6.5 eV with the energy resolution of 10 meV, using a phase modulated spectroscopic ellipsometer (UVISEL, Jobyn Yvon) at angles of incidence variable in the range 55−75°. Ellipsometry measures the ratio, ρ, of the Fresnel reflection coefficient of the p-polarized (parallel to the plane of incidence of the linearly polarized light beam) and s-polarized (perpendicular to the plane of incidence) light reflected from the surface through the ellipsometric angles Ψ and Δ defined by the equation $\rho = \tan\Psi \exp(i\Delta)$, where $\tan\Psi = |E_p|/|E_s|$ and $\Delta = \delta_p - \delta_s$ represent the amplitude and phase variation of the electric field vector associated with the light electromagnetic wave. ρ and, hence, Ψ and Δ are related to the film pseudodielectric function, $\langle\epsilon\rangle = \langle\epsilon_1\rangle + i\langle\epsilon_2\rangle$, through the equation $\langle\epsilon\rangle = \sin^2\phi[1 + \tan^2\phi\,(1-\rho)^2/(1+\rho)^2]$, where ϕ is the angle of incidence.

SE spectra of the pseudodielectric function, $\langle\epsilon\rangle = \langle\epsilon_1\rangle + i\langle\epsilon_2\rangle$, were analyzed by using a multilayer model consisting of substrate−interface−CCTO bulk-surface roughness. The CCTO dielectric function was modeled by using an ensemble of Lorentzian oscillators[22,23]

$$\epsilon = \epsilon_1 + i\epsilon_2 = \epsilon_\infty + \sum_j \frac{A_j\omega_j^2}{\omega_j^2 - \omega^2 - i\gamma_j\omega}$$

where ϵ_∞ is the high-frequency dielectric constant, and ω_j, γ_j, and A_j are the frequency, width and strength of the j oscillator. The surface roughness was modeled by using a mixture of 50% of bulk CCTO and 50% of voids dielectric functions. Through the analysis of SE spectra, the thickness and dielectric function of the CCTO films were derived. For the analysis of data a regression approach was used, building a model representing the sample structure and calculating Ψ and Δ for that model for N photon energies. The calculated values are compared with the measured data in a fit routine that, using a Levenberg−Marquadt algorithm by varying film thickness and optical constants, minimizes the mean squared error, χ^2, defined as

$$\chi^2 = \frac{1}{2N-P-1}\sum_{i=1}^{N}\frac{(\langle\epsilon_{1,\mathrm{exp}}\rangle_i - \langle\epsilon_{1,cal}\rangle_i)^2}{\sigma_{1,i}^2} + \frac{(\langle\epsilon_{2,\mathrm{exp}}\rangle_i - \langle\epsilon_{2,\mathrm{cal}}\rangle_i)^2}{\sigma_{2,i}^2}$$

where N is the total number of data points, P is the number of fitted parameters, $\langle\epsilon_{1,\mathrm{exp}}\rangle$, $\langle\epsilon_{1,\mathrm{cal}}\rangle$ and $\langle\epsilon_{2,\mathrm{exp}}\rangle$, $\langle\epsilon_{2,\mathrm{cal}}\rangle$ represent the experimental and calculated real and imaginary parts of the pseudodielectric function, and σ_i is the error of each measured quantity.

Finally, capacitance−voltage ($C-V$) measurements on MIM capacitors (Pt/CCTO/Pt/TiN/SiO_2/Si) have been carried out adopting the Terman method on circular devices of different areas having radius from 25 to 50 μm. The $C-V$ characteristics have been measured as a function of temperature at 1 MHz from 80 to 450 K in a low noise probe station, using a $C-V$ plotter (HP4284A).

Results and Discussion

Molten Precursor Mixture. The present and up-to-date "unique" MOCVD process for the fabrication of CCTO thin films relies upon a novel approach based on the use of a molten multicomponent precursor source in a horizontal hot-wall reactor. The multicomponent precursor source consists of a homogeneous mixture of $Ca(hfa)_2$·tetraglyme, $Cu(tmhd)_2$, and

TABLE 1: Vaporization Intervals (°C) and Residue Left (%) at 450 °C of Individual Precursors and Their Ca:Cu:Ti (1:1:3) Molten Mixture

	$Ti(tmhd)_2(O\text{-}iPr)_2$	$Cu(tmhd)_2$	$Ca(hfa)_2$tetraglyme	Ca:Ti:Cu mixture
−20 Torr				
vaporization interval	100−190 °C	90−190 °C	100−190 °C	100−190 °C
residue left	1%	1%	1%	1%
−760 Torr				
vaporization interval	150−280 °C	150−230 °C	160−260 °C	200−250 °C
residue left	4%	3%	5%	3%

$Ti(tmhd)_2(O\text{-}iPr)_2$ [Htmhd = 2,2,6,6-tetramethyl-3,5-heptandione; O-*i*Pr = isopropoxide; Hhfa = 1,1,1,5,5,5-hexafluoro-2,4-pentanedione; tetraglyme = 2,5,8,11,14-pentaoxapentadecane] in a 1:1:3 stoichiometric ratio. Although we already reported on both Ca and Cu precursors characterization,[24,25] and the Ti precursor has been widely investigated,[26,27] the comparative study of all the individual precursors and an accurate characterization of the molten multicomponent mixture remains essential to test the real potentialities for this specific application. Thus, the thermal behaviors of $Ca(hfa)_2$·tetraglyme, $Cu(tmhd)_2$, and $Ti(tmhd)_2(O\text{-}iPr)_2$ individual precursors and of the Ca:Cu:Ti 1:1:3 mixture have been investigated by thermogravimetric (TG) measurements and differential scanning calorimetry (DSC).

The dynamic thermogravimentric curves have been carried out at 20 and 760 Torr under purified nitrogen flow. The TG measurements of the molten mixture (Figure 1a) indicate that sublimation/evaporation occurs in a single step independently from the total pressure. In Table 1 intervals of vaporization temperatures of all the precursors under the two different pressures are summarized and compared with data of the molten precursor mixture. There is clear evidence that in all cases lower temperature intervals and smaller residues occur under reduced pressure (20 Torr). In fact, the TG curve of the mixture at reduced pressure shows a single step in the 100−190 °C temperature range associated with vaporization and a 1% residue at 450 °C, while the atmospheric pressure TG curve indicates that the molten mixture quantitatively evaporates in a higher temperature range.

Further insights have been obtained from isothermal thermogravimetric (ITG) analyses under reduced pressure (20 Torr), i.e., under experimental conditions similar to those used in the MOCVD process. The mass loss vs time dependencies have been recorded in the 90−140 °C temperature range under nitrogen flow. A linear behavior has been found for all the single precursors in the entire investigated temperature range. The ITG curves (Figure 1b) of the molten precursor mixture show that vaporization rates remain constant under constant temperature and that the values linearly increase upon increasing the temperature in the 90−120 °C range. At temperatures higher than 120 °C a nonlinear behavior is observed thus suggesting that contributions of individual precursors may prevail giving rise to differential vaporization rates. However, at temperatures higher than 100 °C the precursor mixture possesses a high volatility and, therefore, it can be safely used up to 120 °C.

Moreover, apparent molar enthalpies of sublimation/evaporation processes can be calculated from the slope of the Arrhenius plots (Figure 1c). In Table 2 the apparent activation energy values of all the precursors and of the molten mixture are compared. In the 90−130 °C interval, the apparent activation energies of vaporization have been estimated to be 69 ± 2, 92 ± 3, and 87 ± 3 kJ mol^{-1} for $Ca(hfa)_2$·tetraglyme, $Cu(tmhd)_2$, and $Ti(tmhd)_2(O\text{-}iPr)_2$, respectively. Values reported in the literature for $Cu(tmhd)_2$[28] and $Ti(tmhd)_2(O\text{-}iPr)_2$[26] are higher, 128.1 ± 0.7 and 98.2 ± 2.7 kJ mol^{-1}, respectively. Nevertheless, note that our data have been obtained in a different temperature range and with a completely different process, which, in this specific case, may not occur under pseudoequilibrium condition. Moreover, in the case of $Ti(tmhd)_2(O\text{-}iPr)_2$ the literature values have been calculated on $Ti(tmhd)_2(O\text{-}iPr)_2$ precursor synthesized by an original technique[26] and its melting point (155−157 °C) does not agree with the value reported for the commercial product presently used.

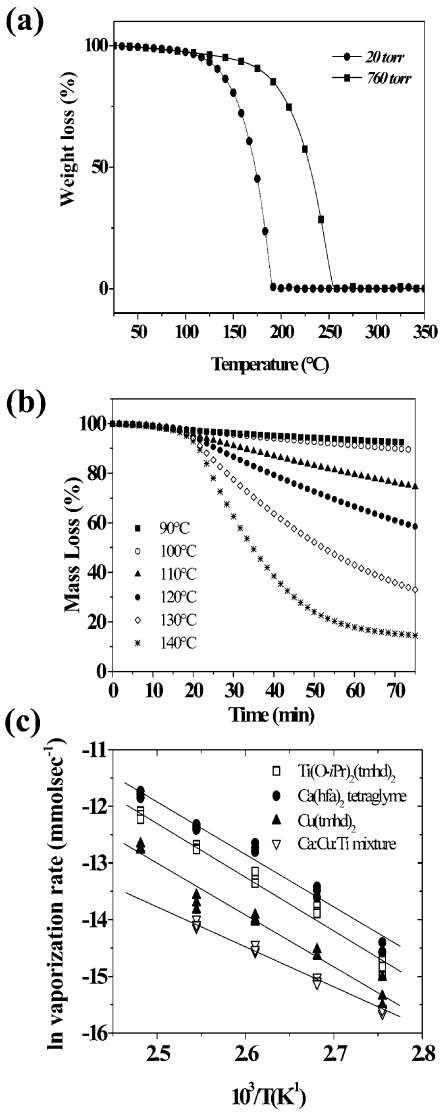

Figure 1. TG curves at different pressures (a), weight change with time at constant temperature (b), and Arrhenius diagram (c) for the $Ca(hfa)_2$·tetraglyme, $Cu(tmhd)_2$, and $Ti(tmhd)_2(O\text{-}iPr)_2$ 1:1:3 mixture.

TABLE 2: Apparent Activation Vaporization Energy of Individual Precursors and of Their Ca:Cu:Ti (1:1:3) Mixture

	$Ti(tmhd)_2$-$(O\text{-}iPr)_2$	$Cu(tmhd)_2$	$Ca(hfa)_2$-tetraglyme	Ca:Cu:Ti mixture
E_{att} (kJ mol^{-1})	87 ± 3	92 ± 3	69 ± 2	63 ± 3

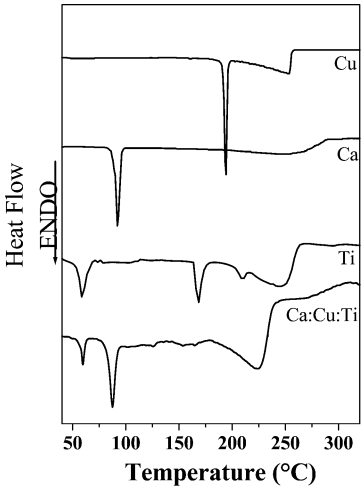

Figure 2. DSC curves of the pure Ca(hfa)$_2$·tetraglyme, Cu(tmhd)$_2$, and Ti(tmhd)$_2$(O-*i*Pr)$_2$ precursors compared to the curve of their 1:1:3 mixture.

Great attention should be devoted to the Arrhenius plot of the Ca:Cu:Ti mixture in the 90−120 °C temperature range, where the trend fits the canonical behavior of a good, thermally stable "single" precursor. The vaporization apparent activation energy of the molten mixture vaporization is 63 ± 3 kJ mol^{-1} thus indicating that the evaporation occurs quite easily.

Other useful information on the properties of the molten precursor mixture have been obtained from calorimetric data (Figure 2) of individual precursors compared to those of the molten mixture. Calcium and copper precursors show two endothermic DSC peaks due to melting (94.0 and 198.6 °C, respectively) and to evaporation from melts (200−280 and 220−250 °C). The DSC curve for the Ti(tmhd)$_2$(O-*i*Pr)$_2$ precursor shows two sharp endothermic peaks associated with two crystal change structures at 60 and 164 °C, while the higher temperature peaks at 205 and 244 °C are related to melting and evaporation, respectively.[29] The molten Ca:Cu:Ti mixture shows a small temperature peak (60 °C) associated with the first structure change of the Ti(tmhd)$_2$(O-*i*Pr)$_2$ component and an higher temperature peak at 88.7 °C associated with the Ca(hfa)$_2$·tetraglyme melting. Some small features in the 120−175 °C range may be related to dissolution of Ti and Cu components. Finally a broad endothermic peak in the 180−240 °C temperature range is associated with the mixture vaporization from melt. Note that the endothermic peak expected for the Cu(tmhd)$_2$ and Ti(tmhd)$_2$(O-*i*Pr)$_2$ melting is not observed. Therefore, the Ca(hfa)$_2$·tetraglyme precursor acts, on melting, as a solvent for the Ti and Cu sources and forms a homogeneous mixture of the three precursors.

The present investigation points to appropriate thermal characteristics of the molten mixture, which can be surely considered an interesting multielement source for MOCVD applications.

To conclude, the present thermal investigation on the Ca:Cu:Ti mixture suggests that it can be used as a single multicomponent precursor since it allows a stable evaporation from the melt with a vaporization rate that remains constant during the vaporization time up to 120 °C.

Film Growth and Characterization. Depositions have been carried out on 10 × 10 mm^2 $SrTiO_3$(100), $LaAlO_3$(100), and Pt/TiO_2/SiO_2/Si(100) substrates through a two-step in situ MOCVD process, namely sequential deposition and annealing steps have been carried out in a hot wall reactor.

In accordance with literature data,[13] films grown on $SrTiO_3$(100) substrates mainly consist of $CaTiO_3$(100) films. In fact, as observed in the XRD patterns (Figure 3a) the principal peaks can be related to the formation of epitaxial $CaTiO_3$(100) films and only a few peaks (centered at 34.4°, 42.5°, and 49.5°) of low intensity correspond to the CCTO phase. The preferential formation of the $CaTiO_3$ phase can be explained on the basis of the larger lattice mismatch (≈6%) between CCTO and $SrTiO_3$ than that between $CaTiO_3$ and the $SrTiO_3$ substrate (0.4%).

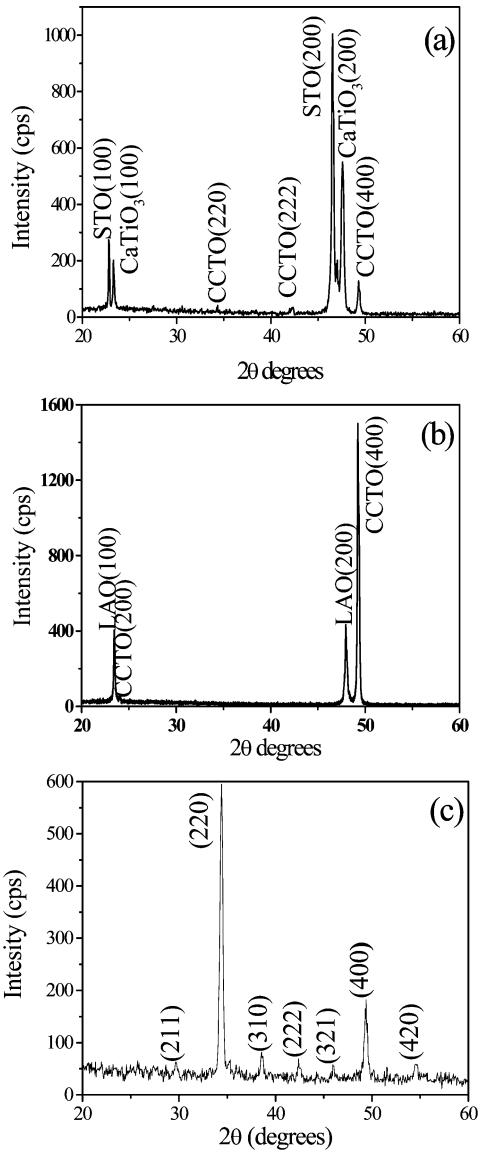

Figure 3. $\theta-2\theta$ XRD patterns of films deposited on (a) $SrTiO_3$(100), (b) $LaAlO_3$(100), and (c) Pt/TiO_2/SiO_2/Si substrate.

In regards to films deposited on $LaAlO_3$ substrates, the possibility to grow pure epitaxial CCTO films has been widely demonstrated.[12−15,19] In Figure 3b is shown the typical XRD pattern for CCTO samples deposited on $LaAlO_3$(100). By contrast to the previous case, the deposited CCTO films are pure and completely (100) oriented.

In the case of the technological Pt/TiO_2/SiO_2/Si(100) substrate, the XRD pattern (Figure 3c) shows the 211, 220, 310, 222, 321, 400, and 420 reflections with relative intensities comparable to that of the CCTO powder pattern (International Center Diffraction Data No. 21-140) thus pointing out the polycrystalline nature of the annealed films.[20] In the case of the present MOCVD process, it can be concluded that the pure polycrystalline CCTO phase is obtained without any phase impurity (i.e. pyrochlore) as reported in some cases for the PVD growth.[16]

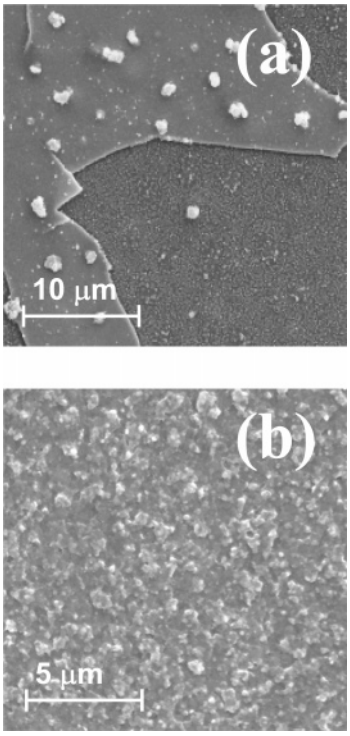

Figure 4. SEM images of CCTO films annealed at 900 (a) and (b) 750 °C for 120 min.

Nevertheless, the in situ annealing at 900 °C has proven not well suited for the $Pt/TiO_2/SiO_2/Si(100)$ substrate that does not appear sufficiently stable at this high temperature. In fact, SEM images show cracks on the entire surface (Figure 4a). On the other hand, simultaneous experiments carried out on $LaAlO_3(100)$ substrates adopting lower annealing temperatures (750 °C) yield CCTO films whose $\theta-2\theta$ patterns clearly indicate a *c*-axis orientation, even though their in-plane and out-of-plane alignments indicate a lower degree of epitaxy with respect to the 900 °C deposited samples. In particular, the out-of-plane orientation spread of CCTO (100) films (estimated from fwhm of the rocking curve of the 400 CCTO reflection) increases from 0.6° to around 2° for films annealed at 900 and 750 °C, respectively. Therefore, the annealings of Ca−Cu−Ti matrices on $Pt/TiO_2/SiO_2/Si(100)$ substrate have been carried out at 750 °C for 120 and 30 min, considering that this temperature does not significantly affect the structural properties of the deposited CCTO films.

SEM images of 750 °C annealed samples on the $Pt/TiO_2/SiO_2/Si(100)$ substrate (Figure 4b) show homogeneous surfaces with no cracks in both cases. There are large rounded grains of about 100 nm average size, while for 30 min annealing time the mean grain size is about 50 nm. Cross-section SEM images show dense CCTO thin films. The film thickness is approximately 900 nm for 120 min deposition, thus implying a 7 nm/min mean growth rate.

The atomic composition of the deposited films has been evaluated by Energy Dispersive X-ray analyses (EDX). EDX data of both as-deposited and annealed films always agree with the expected chemical composition. EDX analyses of several selected areas (50 μm × 50 μm) indicate that almost constant $1 \pm 0.05:2.6 \pm 0.05:4.3 \pm 0.05$ stoichiometries are maintained over the whole 10×10 mm^2 surface. The Ca Kα and Kβ peaks are observed at 3.690 and 4.010 keV, the Ti L lines are spread in the 4.400−5.100 keV range, and the Cu Kα and Kβ peaks are observed at 8.040 and 8.900 keV, respectively. The Pt M lines are centered at 2.270 keV. In addition, the EDX measurements adopting the windowless detector show the O Kα peak at 0.520 keV, while the absence of the peak at 0.670 keV rules out any F contamination in the films within the detection limits of the EDX technique (~1% for F).

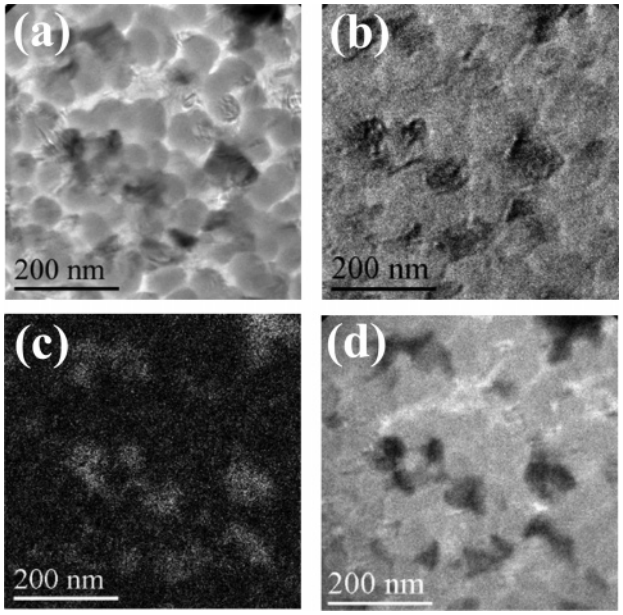

Figure 5. Chemical maps of an as-deposited CCTO film performed by energy-filtered transmission electron microscopy (EF-TEM): (a) zero loss image; (b) energy-filtered calcium map obtained by the Ca_K 232 eV edge; (c) energy-filtered copper map obtained by the Cu_M 931 eV edge showing the presence of crystalline copper rich grains; and (d) energy-filtered titanium map obtained by the Ti_L 99 eV. All the chemical maps have been acquired by the three windows method.

Better insight on the composition of deposited films has been provided by Energy Filtered Transmission Electron Microscopy (EF-TEM). Thus, energy filtered bidimensional chemical maps have been determined for all the components of Ca:Cu:Ti matrix deposited at 600 °C (Figure 5). The zero loss energy image clearly shows the presence of some crystalline grains embedded in an amorphous matrix. The chemical nature of these crystalline grains has been determined by the chemical maps of each CCTO component. By comparison of the Ca, Cu, Ti, and O signal intensities it can be concluded that the crystalline grains likely consist of copper oxide grains. In fact, the intensity of the copper signal increases in correspondence with crystalline grains. On the other hand, Ti, Ca, and O signals are well distributed all over the matrix. The EF-TEM maps of the annealed samples are shown in Figure 6. In this case no phase separation is evident and the three elements are uniformly distributed all over the sample.

Dielectric Characterization. Optical characterization has been performed for samples grown on both $LaAlO_3$ and $Pt/TiO_2/SiO_2/Si(100)$ substrates. Preliminary data have been communicated in ref 20. Figure 7 shows the spectra of the refractive index and of the extinction coefficient (related to the absorption coefficient $\alpha = 4\pi k/\lambda$, where λ is the wavelength of light) derived, after correction for surface roughness effects, for CCTO films obtained under various conditions of deposition temperature and annealing time. It is well-known that interband electronic transitions and free carriers are responsible for the material optical properties.[30] In the present case, peaks observed in the extinction coefficient spectra at approximately 4 eV may be associated with electronic transitions to unoccupied conduction band states, which are primarily Ti 3d-like (mainly t_{2g} states), while peaks at approximately 5 eV may be associated

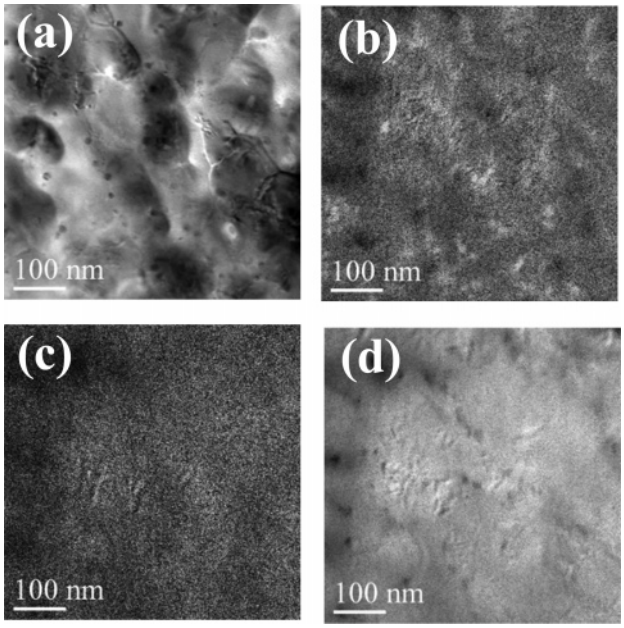

Figure 6. Chemical maps of an annealed CCTO film performed by energy-filtered transmission electron microscopy (EF-TEM): (a) zero loss image; (b) energy-filtered calcium map obtained by the Ca_K 232 eV edge; (c) energy-filtered copper map obtained by the Cu_M 931 eV edge showing the presence of crystalline copper rich grains; and (d) energy-filtered titanium map obtained by the Ti_L 99 eV edge.

with e_g states.[20, 31] At photon energies below 2 eV, some of the extinction coefficient spectra show a feature likely due to free carrier absorption.

The spectra of the extinction coefficient in the region above 2 eV of the various samples qualitatively differ in amplitude. This suggests that differences in this region are due to the amount of polarizable material per unit volume, or void fraction. This is also supported by the AFM images and grain height line profiles shown at the bottom of the same figure, which show a different grain size for the various films.

Data in Figure 7 show that the larger the grain size, the greater the amplitude of the extinction coefficient spectra in the energy range above 2 eV and the higher the dispersion in spectra of the refractive index. This amplitude increase of spectra and the narrowing of the interband transition critically related to the increase of grain size is a well-known effect largely described in the literature for poly- and microcrystalline silicon.[32] Thus, the above data show that nanostructure and dielectric/optical properties depend on deposition temperature and annealing conditions and that contribution of free carriers is larger for the film with larger grains, and decreases with the decrease of grain size.

It is well-known that CCTO dielectric characteristics are related to conduction regions separated by insulating boundaries. This inhomogeneous electrical structure has been related to oxygen vacancies and/or to cation exchanges on Ti and Cu sites causing insulating barriers within grains.[33]

Our observation suggests that CCTO films consist of semiconducting grains separated by insulating grain boundaries. As in many semiconductor oxides, the semiconducting character is related to oxygen vacancies. The oxygen vacancies and free charges (electrons) within the semiconducting grain might be generated during the annealing treatment, which causes the transition from amorphous to crystalline films (e.g. see Figure 3). When the annealing is performed in oxygen atmosphere, compensation of grain boundaries, which increases their insulating character, might occur since grain boundaries act as a sink-site for oxygen, while the grain core keeps its O-vacancies. It has been reported that compensation of oxygen vacancies (optically readable in the absence of the low-energy absorption in ϵ_2) causes the decrease of the dielectric constant of CCTO films.[34] Therefore, the free-carrier absorption (indication of the oxygen vacancies) and the higher amplitude of the dielectric function (through the Clausius−Mosotti equation) represent reliable indicators of relative qualitative trend of the dielectric constant of films, namely the higher the dielectric function spectra, the greater the dielectric constant.[20]

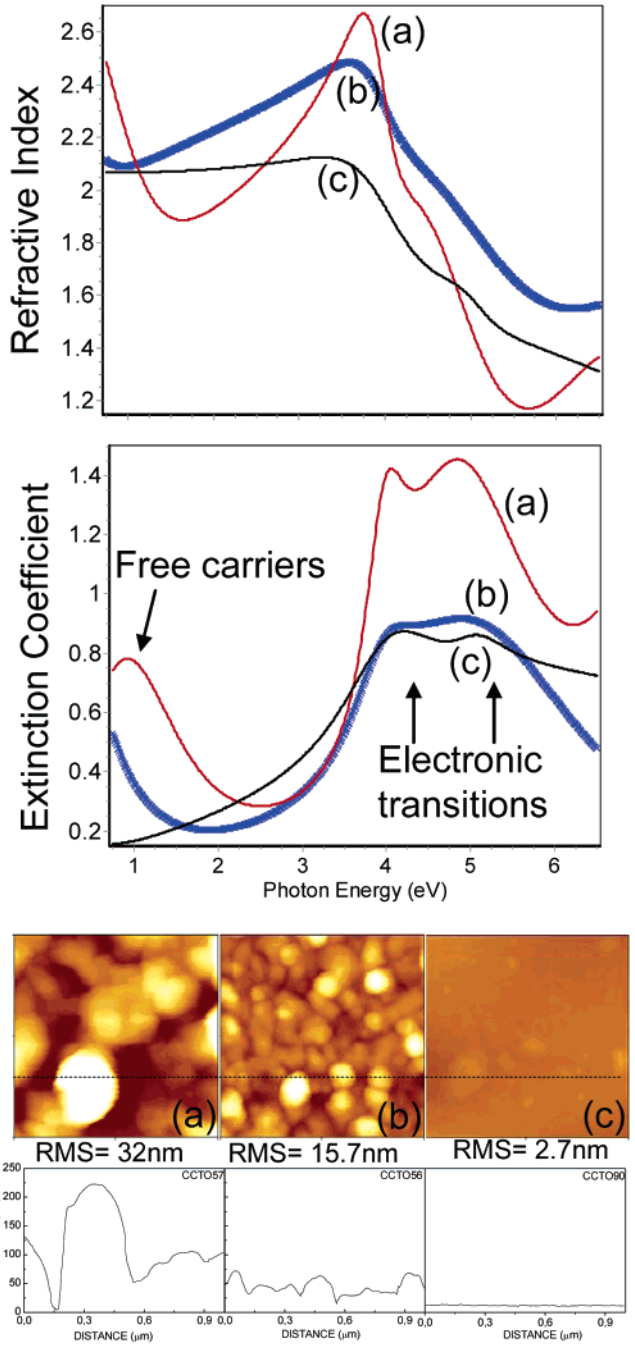

Figure 7. Spectra of the refractive index and of the extinction coefficient derived for CCTO films annealed at 900 °C on $LaAlO_3$ (a) and 750 °C on $Pt/TiO_2/SiO_2/Si$ for 120 min (b) and for 30 min (c). The corresponding 1 μm × 1 μm AFM morphologies, surface roughness (root-mean-square roughness, RMS), and height line profiles are also reported. [Reprinted from Lo Nigro, R.; Malandrino, G.; Toro, R. G.; Losurdo, M.; Bruno, G.; Fragalà, I. L. *J. Am. Chem. Soc.* **2005**, *127*, 13772. Copyright 2005 by American Chemical Society.]

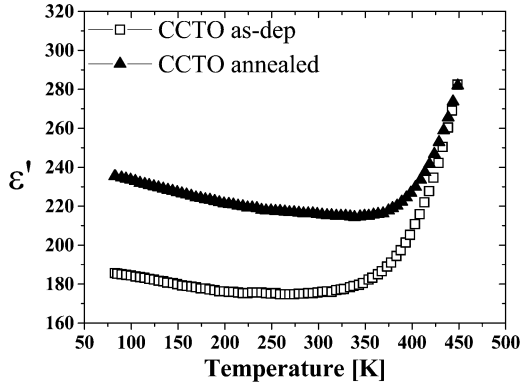

Figure 8. Capacitance−voltage ($C-V$) measurements on MIM capacitors (Pt/CCTO/Pt/TiN/SiO_2/Si) as a function of temperature (50−500 K) at 1 MHz on as-deposited CCTO sample and after an annealing process in oxygen ambient for 8 h.

Finally, preliminary electrical measurements have been recorded on the CCTO films deposited on platinum electrodes. Capacitors have been fabricated as planar metal−insulator−metal (MIM) structures where the CCTO layer has been sandwiched between platinum electrodes. The upper Pt contact has been deposited by sputter deposition and the device fabrication has been obtained by a photolithographic lift-off process.

Figure 8 shows the dielectric constant values at different temperatures (at 1 MHz), expressed as:

$$\epsilon' = \frac{Ct}{\epsilon_0 A}$$

where C is the measured capacitance, t is the CCTO film thickness, ϵ_0 is the vacuum permittivity, and A is the device planar dimension. The dielectric constant values do not significantly change in a wide temperature range (from 80 to 375 K) and we calculated $\epsilon' \approx 180$ for the as-deposited sample. The ϵ' values increase beyond 350 K up to 300. Moreover, it is possible to note an increasing of the dielectric constant values ($\epsilon' \approx 240$) in the 80 to 375 K range after an ex situ annealing process in oxygen ambient for 8 h. These preliminary results seem to point to the mechanism proposed on the basis of ellipsometric data and regarding compensation of oxygen vacancies at grain boundaries as being responsible for the effective dielectric constant value.

However, because this is the first effort on the dielectric measurements of the CCTO films fabricated by MOCVD, the low value of the dielectric constant may be due to several reasons including the defects and/or low film density. Efforts are underway to improve the postannealing steps in oxygen environments, replacing the bottom Pt electrode with a conductive oxide substrate and/or improving the top Pt contact. On the other hand, it has been widely described that the CCTO dielectric properties appears very sensitive to processing, in fact, dielectric constants from 478 to 300 000 have been measured for CCTO ceramics processed in different manners.

Conclusions

In summary, CCTO thin films have been satisfactorily and reproducibly deposited with use of the metal organic chemical vapor deposition technique on $SrTiO_3$(100), $LaAlO_3$(100) single-crystal substrates, and Pt/TiO_2/SiO_2/Si(001) substrates suited for device integration. Comprehensive studies of the related MOCVD process, ranging from the full characterization of the molten precursor mixture to the structural, morphological, and functional properties of deposited films, have been performed.

The present approach takes advantage of a simple multimetal single source, consisting of a homogeneous molten mixture of $Cu(tmhd)_2$, $Ti(tmhd)_2(O\text{-}iPr)_2$, and $Ca(hfa)_2$·tetraglyme in an optimized ratio. The capability of the "second-generation" $Ca(hfa)_2$·tetraglyme precursor to act as a solvent for the other $Cu(tmhd)_2$ and $Ti(tmhd)_2(O\text{-}iPr)_2$ precursors has been exploited and demonstrated. This approach represents an interesting and convenient alternative to the use of various singular sources, in a multielement MOCVD reactor which, of course, requires separate controls of operational parameters (gas flows and sublimation temperatures) of each precursor.

CCTO thin films have been fabricated with an in situ two-step MOCVD process. X-ray diffraction patterns indicate that no pure CCTO films have been formed on $SrTiO_3$(100), epitaxial CCTO films have been obtained on $LaAlO_3$(100), and finally that CCTO films grown on Pt/TiO_2/SiO_2/Si(001) are polycrystalline. EF-TEM measurements indicate homogeneous distribution of the three components over the whole sample area.

To our knowledge, this represents the first comprehensive study of an MOCVD in situ process for fabrication of giant dielectric constant CCTO films on a technologically relevant substrate. Finally, the ellipsometric analysis has revealed the fundamental optical properties and electronic transitions in the near-IR−vis−UV range, and the correlation existing between nanostructure and the optical/dielectric properties of CCTO films. In particular, it has been found that the larger the grain, the higher the dielectric function and the free carrier density.

Acknowledgment. This work has been partially supported by INSTM (Consorzio Interuniversitario Nazionale per la Scienza e Tecnologia dei Materiali) within the PRISMA project and by Europian Commission Union under the project NUOTO (New materials with Ultrahigh *k* dielectric constant fOr TOmorrow wireless electronics).

References and Notes

(1) Subramanian, M. A.; Li, D.; Duan, N.; Reisner, B. A.; Sleight, A. W. *J. Solid State Chem.* **2000**, *151*, 323.
(2) Ramirez, A. P.; Subramanian, M. A.; Gradel, M.; Blumberg, G.; Li, D.; Vogt, T.; Shapiro, S. M. *Solid State Commun.* **2000**, *115*, 217.
(3) Homes, C. C.; Vogt, T.; Shapiro, S. M.; Wakimoto, S.; Ramirez, A. P. *Science* **2001**, *293*, 673.
(4) Shao, S. F.; Zhang, J. L.; Zheng, P.; Zhang, W. L.; Wang, C. L. *J. Appl. Phys.* **2006**, *99*, 084106.
(5) Adams, T. B.; Sinclair, D. C.; West, A. R. *Adv. Mater.* **2002**, *14*, 1321.
(6) Sinclair, D. C.; Adams, T. B.; Morrison, F. D.; West, A. R. *Appl. Phys. Lett.* **2002**, *80*, 2153.
(7) Cohen, M. H.; Neaton, J. B.; He, L.; Vanderbilt, D. *J. Appl. Phys.* **2003**, *94*, 3299.
(8) He, L.; Neaton, J. B.; Cohen, M. H.; Vanderbilt, D.; Homes, C. C. *Phys. Rev. B* **2002**, *65*, 214112.
(9) He, L.; Neaton, J. B.; Vanderbilt, D.; Cohen, M. H.; Homes, C. C. *Phys. Rev. B* **2003**, *67*, 012103.
(10) Kolev, N.; Bontchev, R. P.; Jacobson, A. J.; Popov, V. N.; Hadjiev, V. G.; Litvinchuck, A. P.; Iliev, M. N. *Phys. Rev. B* **2002**, *66*, 132102.
(11) Homes, C. C.; Vogt, T.; Shapiro, S. M.; Wakimoto, S.; Subramanian, M. A.; Ramirez, A. P. *Phys. Rev. B* **2003**, *67*, 092106.
(12) Lin, Y.; Chen, Y. B.; Garret, T.; Liu, S. W.; Chen, C. L.; Chen, L.; Bontechev, R. P.; Jacobson, A.; Jiang, J. C.; Meletis, E. I.; Horwits, J.; Wu, H. D. *Appl. Phys. Lett.* **2002**, *81*, 631.
(13) Si, W.; Cruz, E. M.; Johnson, P. D.; Barnes, P. W.; Woodward, P.; Ramirez, A. P. *Appl. Phys. Lett.* **2002**, *81*, 2056.
(14) Chen, L.; Chen, C. L.; Lin, Y.; Chen, Y. B.; Chen, X. H.; Bontchev, R. P.; Park, C. Y.; Jacobson, A. J. *Appl. Phys. Lett.* **2003**, *82*, 2317.
(15) Tselev, A.; Brooks, C. M.; Anlage, S. M.; Zheng, H.; Salamanca-Riba, L.; Ramesh, R.; Subramanian, M. A. *Phys. Rew. B* **2004**, *70*, 144101.
(16) Fang, L.; Shen, M. *Thin Solid Films* **2003**, *440*, 60.
(17) Fang, L.; Shen, M.; Cao, W. *J. Appl. Phys.* **2004**, *95*, 6483.
(18) Fang, L.; Shen, M.; Yao, D. *Appl. Phys. A* **2005**, *80*, 1763.

(19) Lo Nigro, R.; Toro, R.; Malandrino, G.; Bettinelli, M.; Speghini, A.; Fragalà, I. L. *Adv. Mater.* **2004**, *16*, 891.

(20) Lo Nigro, R.; Malandrino, G.; Toro, R. G.; Losurdo, M.; Bruno, G.; Fragalà, I. L. *J. Am. Chem. Soc.* **2005**, *127*, 13772.

(21) Malandrino, G.; Castelli, F.; Fragalà, I. L. *Inorg. Chim. Acta* **1994**, *224*, 203.

(22) Djurisić, A. B.; Kwong, C. Y.; Lau, T. W.; Guo, W. L.; Li, E. H.; Liu, Z. T.; Kwok, H. S.; Lam, L. S. M.; Chan, W. K. *Opt. Commun.* **2001**, *205*, 155.

(23) Arwin, H.; Mårtensson, J.; Jansson, R. *Appl. Opt.* **1992**, *31*, 6707.

(24) Malandrino, G.; Perdicaro, L. M. S.; Fragala, I. L.; Testa, A. M.; Fiorani, D. *Chem. Mater.* **2004**, *16*, 608.

(25) Malandrino, G.; Perdicaro, L. M. S.; Condorelli, G. G.; Cassinese, A.; Prigiobbo, A.; Fragala, I. L. *Chem. Vap. Dep.* **2005**, *11*, 381.

(26) Turgambaeva, A. E.; Krisyuk, V. V.; Sysoev, S. V.; Igumenov, I. K. *Chem Vap. Dep.* **2001**, *7*, 121.

(27) Ryu, H.-K.; Heo, J. S.; Cho, S.-I.; Moon, S. H. *J. Electrochem. Soc.* **1999**, *146*, 1117.

(28) Ribeiro da Silva, M. A. V.; Monte, M. J. S.; Huinink, J. *J. Chem. Thermodyn.* **1995**, *27*, 175.

(29) Chen, I. S.; Roeder, J. F.; Glassman, T. E.; Baum, T. H. *Chem. Mater.* **1999**, *11*, 209.

(30) Losurdo, M. *Thin Solid Films* **2004**, *301*, 455.

(31) He, L.; Neaton, J. B.; Cohen, M. H.; Vanderbilt, D.; Homes, C. C. *Phys. Rev. B* **2005**, *65*, 214112.

(32) Jellison, G. E. In *Handbook of Ellipsometry*; Tompkins, H. G., Irene, E. A., Eds.; William Andrew Publishing: Heidelberg, 2005 p 237

(33) Li, J.; Subramanian, M. A.; Rosenfeld, H. D.; Jones, C. Y.; Toby, B. H.; Sleight, A. W. *Chem Mater.* **2004**, *16*, 5223.

(34) Chung, S. Y.; Kim, I. D.; Kang, S. J. *Nat. Mater.* **2004**, *3*, 774.